JOURNAL OF SPACECRAFT AND ROCKETS
Vol. 37, No. 3, May–June 2000

Base-Drag-Reduction Experiments on the X-33 Linear Aerospike SR-71 Flight Program

Stephen A. Whitmore* and Timothy R. Moes†
NASA Dryden Flight Research Center, Edwards, California 93532

Drag-reduction tests were conducted on the Linear Aerospike SR-71 experiment. The Linear Aerospike SR-71 experiment flight tested a 20% scale model of an X-33 forebody with a linear-aerospike engine mounted at the rear of the body. The entire apparatus was mounted on top of an SR-71 aircraft. This paper suggests a method for reducing base drag by adding surface roughness along the forebody. Calculations show a potential for base-drag reductions of 8–14%. Flight results corroborate the base drag reduction, with actual reductions of 15% in the high-subsonic flight regime. An unexpected result is that drag benefits persist well into the supersonic flight regime. Flight results show no overall net drag reduction. The applied roughness caused forebody pressures to rise and offset base-drag reductions. Apparently, the grit displaced streamlines outward, causing forebody flow compression. Clearly the drag optimization must be modified to include not only the base pressure drag and viscous forebody drag coefficients but must also include the forebody pressure distribution. Because of the mixed experimental results—there was no overall net drag reduction, the existence of an optimal forebody surface roughness must still be proven. Clearly, however, the forebody grit method has been proven as a viable drag-reduction tool.

Nomenclature

A_{base}	= base area of the model, 1.125 m^2
A_{grit}	= wetted area of the surface grit, 3.01 m^2
$C_{D,\text{base}}$	= base-pressure-drag coefficient
$C_{D,\text{forebody}}$	= forebody-pressure-drag coefficient
$C_{D,\text{forebody}}^{(\text{visc})}$	= total-viscous-forebody-drag coefficient (referenced to base area)
C_{Dp}	= total-pressure-drag coefficient for the model
C_{D0}	= zero-lift drag coefficient of the model, from force balance
$C_{D0}^{(p)}$	= zero-lift drag coefficient of the model, from pressures
$\tilde{C}_{D,\text{base}}$	= predicted base-pressure-drag coefficient
$\tilde{C}_{D,\text{base}}^{(0)}$	= predicted base-pressure-drag coefficient, incompressible flow conditions
$c_{f_L}^{(\text{rough})}$	= skin-friction coefficient for rough flat plate
$c_{f_L}^{(\text{smooth})}$	= skin-friction coefficient for smooth flat plate
k_s	= equivalent sand-grain roughness of surface extrusions, m
L	= length of the gritted surface area, 2.0 m
M_{div}	= divergence drag rise Mach number
M_∞	= freestream Mach number
Re_L	= Reynold's number based on length of body
$\Delta C_{D,\text{base}}$	= base-pressure-drag reduction caused by added forebody roughness
$\Delta C_{D,\text{forebody}}^{(\text{visc})}$	= increment in $C_{D,\text{forebody}}^{(\text{visc})}$ caused by added forebody roughness

Introduction

CURRENT proposed configurations for reusable launch vehicles (RLV) like the Lockheed Martin X-33 and Venture-Star have extremely large base areas when compared to previous hypersonic vehicle designs. As a result, base drag, especially in the transonic flight regime, is very large. The unique configuration of the Venture Star RLV, with its very large base area and relatively low forebody drag, offers the potential for a very high payoff in base-drag reduction. If the transonic base-drag coefficient of the Venture-Star can be reduced by only 5%, then the potential subsonic and transonic (where most of the fuel is burned) drag savings is approximately 30,000–40,000 lb. Such a reduction in fuel expenditure would dramatically increase the payload capability of the vehicle.

Based on the preceding reasoning, a base-drag-reduction experiment was conducted as a part of the Linear Aerospike SR-71 (LASRE) flight program, which has recently concluded testing at the NASA Dryden Flight Research Center. This drag-reduction experiment attempted to reduce the base drag, and the overall vehicle drag, by increasing the forebody skin friction. In this experiment the forebody skin friction was modified by increasing the effective roughness of the forebody surface. The basic approach of the drag-reduction experiment is to thicken the boundary layer at the aft end of the vehicle and provide an insulating layer that reduces the vacuum-pump effect on the highly separated base area. This report presents the results of the base-drag-reduction experiment and compares the resulting drag coefficient values to the X-33 wind-tunnel database. A more comprehensive discussion of the analytical methods used in this analysis is presented by Whitmore and Moes.[1]

LASRE Flight Experiment

The LASRE experiment[2] consisted of a roughly 20% half-span model of an X-33 forebody with a single aerospike rocket engine mounted at the rear. As shown in Fig. 1, the entire test apparatus is mounted on top of an SR-71 aircraft. The model is mounted so that the lateral axis is aligned parallel to the normal axis of the SR-71. This alignment causes the angle of sideslip for the SR-71 to be equivalent to angle of attack for the LASRE model. To achieve better flow quality, a reflection plane was mounted between the SR-71 and the model. The reflection plane shields the model from the SR-71 flowfield. Figure 2 presents three-view line drawings of the model and documents the primary geometrical components—the forebody, boat tail, nozzle ramps, base plug, and engine fences. Figure 3 presents a comparison of the LASRE outer mold lines to the X-33 mold lines.

It was intended that LASRE flight test data would be used to define the aerospike engine performance under realistic flight conditions and to determine the rocket-plume interactions with the base area and engine cowlings. Ground-based hot-fire tests of the LASRE engine were performed successfully, and cold-fire flight tests in which the propellants were replaced with inert expendables were

Received 12 February 1999; revision received 2 September 1999; accepted for publication 10 September 1999.

*Aerospace Engineer, P.O. Box 273, Mail Stop D-2228, Aerodynamics Branch. Associate Fellow AIAA.

†Vehicle Aerodynamics Group Leader, P.O. Box 273, Mail Stop D-2228, Aerodynamics Branch. Member AIAA.

also successfully completed. Unfortunately because of hardware difficulties experienced with cold-flow tests with liquid oxygen onboard of the vehicle, safety constraints prevented the engine from ever being hot-fired in flight. The program was terminated without successfully completing this final test objective.

Instrumentation

To measure performance of the Linear Aerospike engine under a variety of flight conditions, the model was mounted to the SR-71 with a pylon that was instrumented with eight load cells oriented to allow a six-degree-of-freedommeasurement of the total forces and moments. A schematic of the force balance mounted to the LASRE pylon is shown in Fig. 4. A calibration tensor was used to compute the axial, normal, and side loads, and pitch, roll, and yaw moments acting at the balance. To determine the true aerodynamic forces acting on the model, it is necessary to remove the centrifugal force and vehicle accelerations acting at the model center of gravity. The vehicle accelerations and angular rates were obtained from strapdown sensors located near the SR-71 center of gravity. The corrected data were normalized to give force coefficients using the dynamic pressure measurement obtained from the SR-71's onboard air data system.

The model was also instrumented with surface pressure ports on the forebody, boat tail, base, engine ramps, and the lower engine fence. These surface pressure ports allowed the model pressure drag to be measured by numerically integrating the surface pressure distributions. A total of 95 ports were distributed on the forebody and boat tail. The approximate locations of the forebody and boat tail ports are presented schematically on Fig. 2. An additional 60 ports were located in the engine base area, with 20 pressure ports located on the left engine ramp, 22 ports on the right engine ramp, 16 ports on the engine base plug, and 2 ports were located on the trailing edge of the lower engine fence. The approximate locations of the engine pressure ports are also presented on Fig. 2. The model pressure data were sensed using electronically scanned pressure (ESP) modules. Because of pressures ranges expected during aerospike engine hot-fire tests, engine ramp and fence pressures were sensed using ±50 psi differential pressure sensors; all other surface pressure

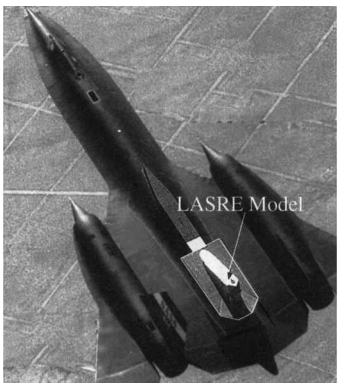

Fig. 1 LASRE experiment mounted atop the SR-71.

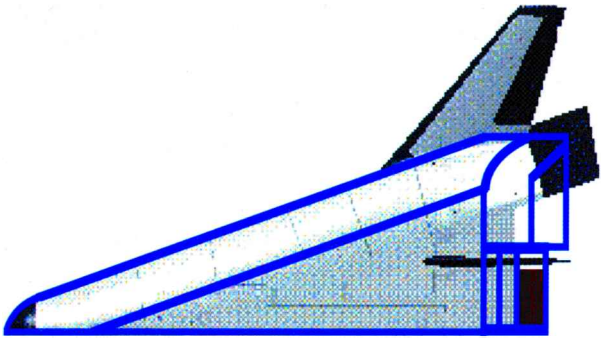

Fig. 3 Comparison of the LASRE outer mold lines to the X-33.

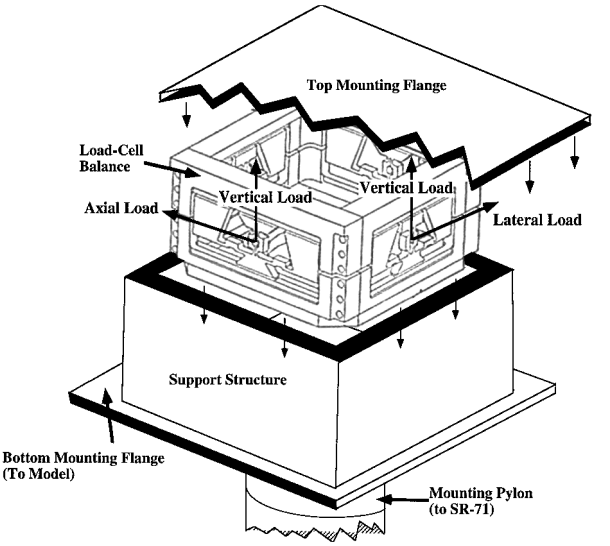

Fig. 4 Schematic of the LASRE force balance.

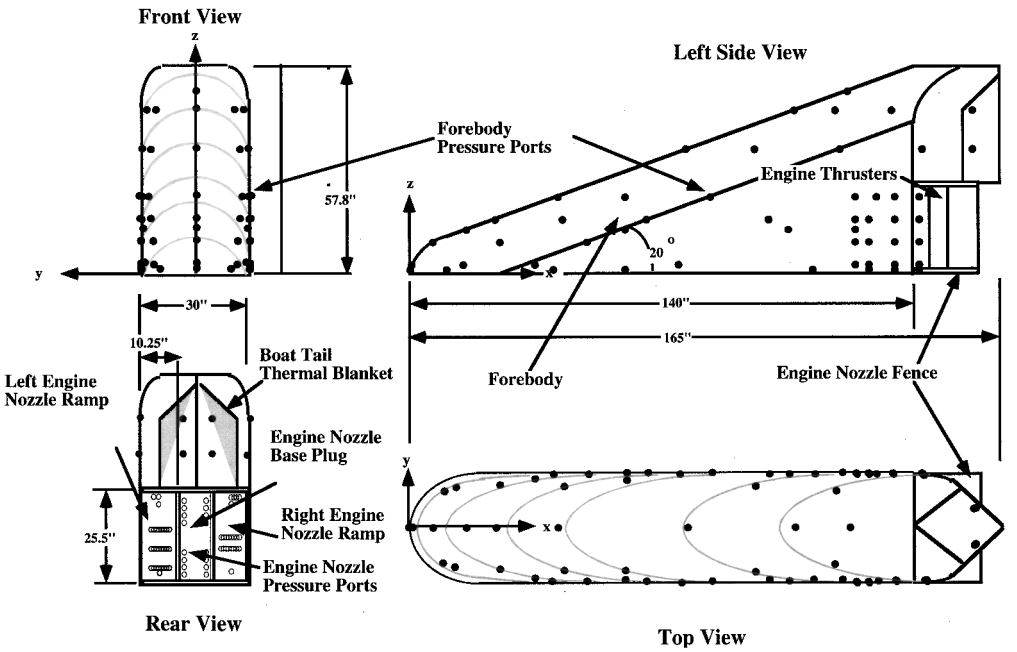

Fig. 2 LASRE test model.

measurements were made using ±10 ESPs. All ESPs were referenced to a highly accurate 0–38 psia 20-bit digital pressure transducer. The reference pressure was added to the differential ESP readings to determine absolute local pressure reading. Temperature environments of the ESPs were controlled using heater blankets.

The numerical integration of the surface pressures to obtain pressure-drag coefficients was performed for each of six geometrical components on the model: 1) the model forebody aft to 140 in. behind the nose tip, 2) the engine nozzle left ramp, 3) the engine nozzle right ramp, 4) the engine nozzle base plug, 5) the LASRE model boat tail, and 6) the lower engine fence. Once the individual pressure-drag coefficients of each geometrical component were determined, the base-pressure-drag coefficient was calculated as the area-weighted average of the nozzle, boat tail, and engine fence pressure coefficients. The total model pressure drag was calculated as the area-weighted average of the base and forebody pressure-drag coefficients.

All onboard analog instrumentation were sampled using 12-bit pulse-code modulation, telemetered to the ground, and recorded for postflight analysis. The air-data parameters, force balance load cell data, and pressure measurements were sampled and recorded at 50 samples per second (sps). Onboard accelerometer and rate-gyro readings were sampled and recorded at 200 sps. The accelerometer and rate-gyro data were antialiased using analog filters with cutoff frequencies at 40 Hz. To reduce the effects of stochastic noise elements caused by aerodynamic and structural interactions of the SR-71 on the LASRE model, all of the data used in the drag analysis were postflight low-pass filtered at 0.5 Hz and then decimated to 1.0 sps. Filter latency was accounted for by time skewing the data after filtering. This procedure also served to mitigate potential aliasing problems. The processed data were corrected for zero offsets using preflight and postflight zero-tare data.

Flight Profiles

Early in the program level altitude subsonic-to-supersonic accelerations were flown for envelope expansion and flutter clearance. Once the flight envelope clearance was obtained, a more fuel-efficient "dipsy" maneuver was used to accelerate through the transonic drag rise. The dipsy maneuver began at 28,000 ft and Mach 0.9, where the pilot put the aircraft into a slight dive to get through the transonic drag rise and then leveled the aircraft at approximately Mach 1.07 and 25,000 ft—the minimum altitude cleared for transonic flight. The aircraft would continue to accelerate at 25,000 ft until it obtained an equivalent airspeed of 450 kn. At this point the pilot would initiate a constant equivalent airspeed climb to the desired Mach number. Structural load restrictions on the LASRE experiment required that the angle of sideslip, equivalent to angle of attack in the model axis, be restricted to less that 2 deg. Because of this restriction, all of the drag data presented in this paper are essentially for the zero-lift flight condition, C_{D_0}. Additionally, throughout the remainder of this paper all drag coefficient data are referenced to the base area of the LASRE model.

Accuracy Analysis Methods

Because of the heavy filtering applied to all of the data sources, it was believed that an analytical estimate of the drag coefficient accuracies based on root-sum-square analyses would be far too conservative. Instead, the resolution and accuracy of the drag measurements were determined empirically. Drag coefficient data obtained from different flight profiles were examined for resolution and repeatability. The absolute accuracies of the drag coefficients were estimated by comparing the force balance-measured total drag coefficients against the sum of the integrated surface pressure drag and a calculation of the viscous frictional forces acting on the model. For the accuracy analysis only data for a clean LASRE configuration, that is, a configuration without added forebody surface roughness, were analyzed.

Data derived from four typical clean configuration flight maneuvers are used here to illustrate the resolution, repeatability, and accuracy of the measurements. Figure 5 shows the overall balance-derived drag coefficient C_{D_0} plotted as a function of Mach number. Values of the pressure-derived-drag coefficient C_{D_p}, the base-pressure-drag coefficient $C_{D,\text{base}}$, and forebody-pressure-drag coefficient $C_{D,\text{forebody}}$ are also plotted. Maximum flight-to-flight drag coefficient variations of less than 0.008 were observed. In the subsonic flight regime base-pressure drag is relatively constant at approximately 0.38. Also, in the subsonic flight regime there is considerable forebody suction (negative pressure-drag coefficient) and the base-pressure drag actually accounts for approximately 125% of the overall model drag! Once the divergence drag rise Mach number M_{div}—approximately 0.90—is reached, compressibility effects dominate, and base-pressure-drag coefficient rises

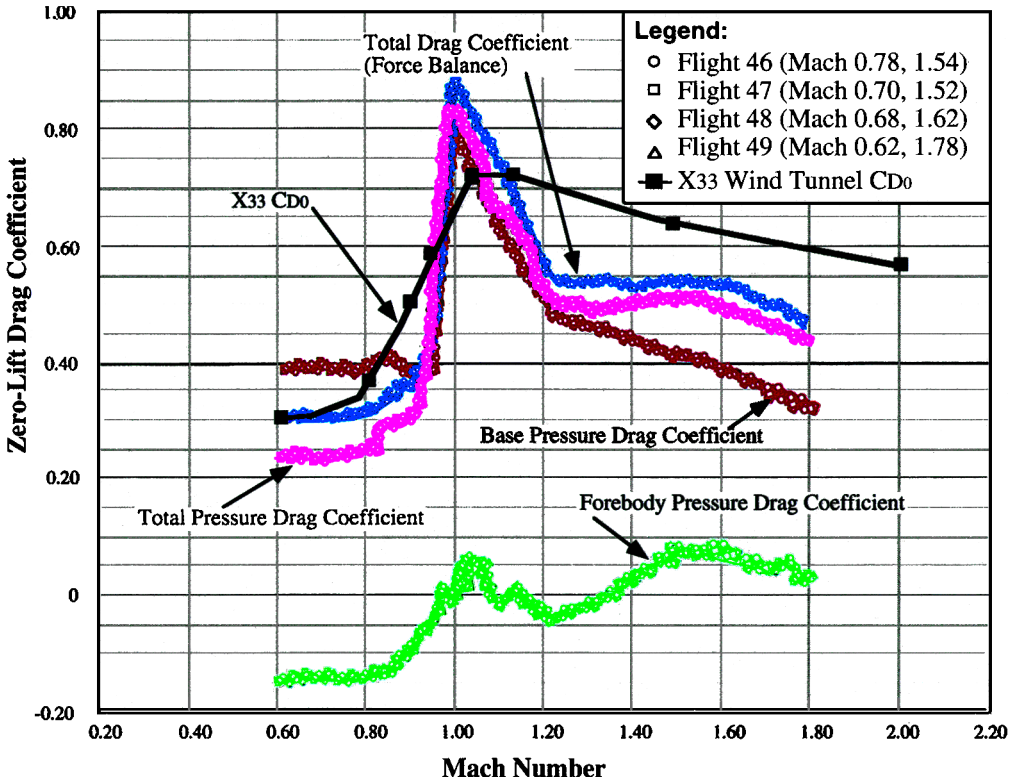

Fig. 5 Comparison of force balance derived drag coefficient to base, forebody, and total-pressure-drag coefficients.

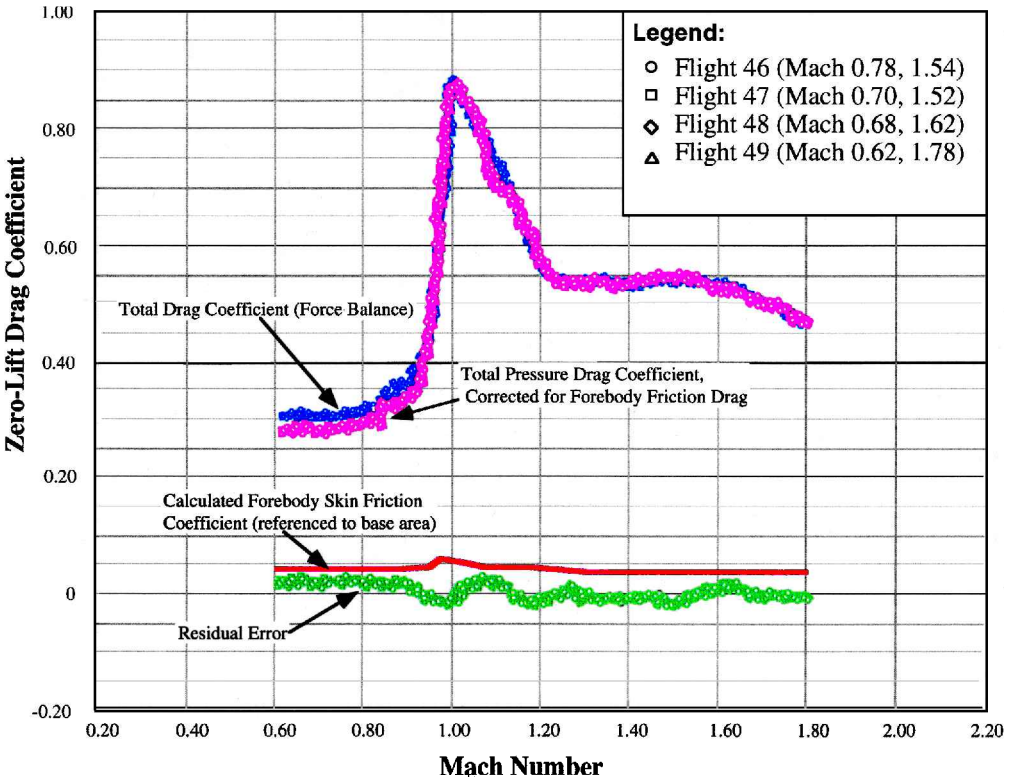

Fig. 6 Comparison of force balance derived drag coefficient to total-pressure-drag coefficient corrected for forebody friction drag.

rapidly. Approximately 80% of the transonic drag rise can be attributed to compressibility effects on base-pressure drag. These data clearly support the earlier assertion that base-pressure drag dominates the overall model drag. Also, clearly the flight-to-flight repeatability and resolution of the drag measurements are excellent.

For comparison purposes wind-tunnel derived values for the X-33 C_{D_0} are also plotted on Fig. 5. The large transonic drag rise observed on the flight data does not show up as dramatically on the X-33 wind-tunnel predictions. It is likely that the observed transonic drag difference is an effect of the differences in fixtures used to mount the wind tunnel and flight models. Conceivably, the mounting of the LASRE model near the reflection plane could have induced significant boundary-layer/shock-wave interactions that were not present in the X-33 wind-tunnel tests. Clear reasons for the large transonic differences are unresolved at this time.

Absolute accuracy estimates for the drag coefficients are obtained by comparing the total drag coefficient obtained from the force balance C_{D_0}, against the total-pressure-drag coefficient corrected for viscous forebody drag $C_{D_0}^{(p)}$. For the LASRE model the viscous forebody drag coefficient $C_{D,\text{forebody}}^{(\text{visc})}$, has two principal components: 1) the forebody skin-friction drag and 2) the ram drag resulting from a small (0.025 m) gap between the lower side of the model and the reflection plane. Forebody skin friction was evaluated by numerically solving the nonlinear Schoenherr equation[3] for the skin-friction drag coefficient. The ram drag is calculated by performing a one-dimensional momentum loss calculation in the axial direction along the gap area. The comparison of C_{D_0} and $C_{D_0}^{(p)}$ is presented in Fig. 6 along with the residual between C_{D_0} and $C_{D_0}^{(p)}$. The estimate of $C_{D,\text{forebody}}^{(\text{visc})}$ is also plotted on Fig. 6. The largest residual magnitude—approximately 0.025—occurs for subsonic Mach numbers less than 0.9. Supersonically, the residual magnitude is always less than 0.005. Because the estimates of C_{D_0} and $C_{D_0}^{(p)}$ were derived independently, assuming that the errors in C_{D_0} and $C_{D_0}^{(p)}$ are approximately equal, then the residual curve plotted in Fig. 6 is a two-σ measure of the overall drag coefficient accuracy. In reality, C_{D_0} is likely more accurate than $C_{D_0}^{(p)}$; however, there is no objective means for sorting out the distribution of error between the two data sources.

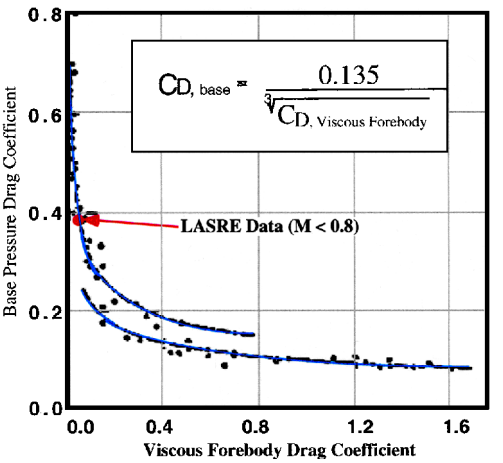

Fig. 7 Correlation of base and viscous-forebody-drag coefficients.

Drag-Reduction Strategy

For blunt-based objects whose base areas are heavily separated, a clear relationship between the base drag and the viscous forebody drag has been demonstrated.[4,5] This trend is presented in Fig. 7 along with subsonic LASRE drag data. Hoerner[4] has fit the trend with the approximate empirical formula:

$$C_{D,\text{base}} = \frac{0.135}{\sqrt[3]{C_{D,\text{forebody}}^{(\text{visc})}}} \tag{1}$$

The trend presented in Fig. 4 shows that as the forebody drag is increased generally the base drag of the projectile tends to decrease. This base-pressure-drag reduction is a result of boundary layer effects at the base of the vehicle. The shear layer caused by the freestream flow rubbing against the separated air in the base region acts as a jet pump and serves to reduce the pressure coefficient in the base area. The surface boundary layer acts as an insulator between the external flow and the dead air at the base. As the forebody drag is increased, the boundary-layer thickness at the aft end

of the forebody increases, reducing the effectiveness of the pumping mechanism, and the base-pressure drag is reduced. Because the LASRE drag data lie on the steep vertical portion of Hoerner's curve, a result of the large base drag, a small increment in the forebody friction drag should result in a relatively large decrease in the base drag. Conceptually, if the added increment in forebody skin drag is optimized with respect to the base drag, then it may be possible to reduce the overall drag of the configuration.

Estimates of the expected base-drag reductions were computed by developing a mathematical model of the LASRE base-drag coefficient, which has $C^{(\text{visc})}_{D,\text{forebody}}$ as a parameter and also accounts for flow compressibility. As mentioned earlier, LASRE base-drag data show that in the subsonic flight regime base drag remains relatively constant until the divergence Mach number of approximately 0.90 is reached. After this Mach number compressibility effects dominate, and the base-drag coefficient rises rapidly. Beyond Mach 1 base drag drops steadily. These trends suggest a base drag compressibility function of the form

$$M_\infty < M_{\text{div}} \Rightarrow \tilde{C}_{D,\text{base}} = \tilde{C}^{(0)}_{D,\text{base}} = \frac{0.135}{\sqrt[3]{C^{(\text{visc})}_{D,\text{forebody}}}}$$

$$M_{\text{div}} \le M_\infty < 1 \Rightarrow \tilde{C}_{D,\text{base}}[M_\infty] = C^{(0)}_{D,\text{base}} \frac{\sqrt{1-M^2_{\text{div}}} + \frac{1}{2}\tilde{C}^{(0)}_{D,\text{base}}\left(1-\sqrt{1-M^2_{\text{div}}}\right)}{\sqrt{1-M^2_\infty} + \frac{1}{2}\tilde{C}^{(0)}_{D,\text{base}}\left(1-\sqrt{1-M^2_\infty}\right)}$$

$$1 < M^2_\infty \Rightarrow \tilde{C}_{D,\text{base}}[M_\infty] = \frac{2\left[\sqrt{1-M^2_{\text{div}}} + \frac{1}{2}\tilde{C}^{(0)}_{D,\text{base}}\left(1-\sqrt{1-M^2_{\text{div}}}\right)\right]}{M^2_\infty} \tag{2}$$

The elements of Eq. (2) are derived from Eq. (1) with modifications for compressibility defined by the Karman–Tsien correction[6] and rules of similarity for transonic flow.[7] The base drag model of Eq. (2) is compared against measured LASRE base drag data in Fig. 6. For such a simple model the agreement is reasonable. Also presented in Fig. 8 are base-drag-reduction increments that would be expected if the viscous forebody drag is increased by 25, 50, 75, and 100%, respectively.

To predict effectiveness of the surface grit, calculations of the increment in $C^{(\text{visc})}_{D,\text{forebody}}$ were performed using the method in Refs. 8 and 9. For a smooth flat plate of length L, the averaged skin-friction coefficient is related to the Reynolds number according to the empirical formula

$$c^{(\text{smooth})}_{f_L} \approx \frac{0.0740}{[Re_L]^{\frac{1}{5}}} \tag{3}$$

When the surface of the plate is roughened, skin friction increases considerably. For a fully rough plate the empirical formula

$$c^{(\text{rough})}_{f_L} = [2.635 + 0.618 \log_e(L/k_s)]^{-2.57} \tag{4}$$

is a good approximation. Using Eqs. (3) and (4), the increment in viscous forebody drag caused by added roughness is calculated as

$$\Delta C^{(\text{visc})}_{D,\text{forebody}} = \left[c^{(\text{rough})}_{f_L} - c^{(\text{smooth})}_{f_L}\right](A_{\text{grit}}/A_{\text{base}}) \tag{5}$$

Based on an estimated range of surface roughness from approximately 5.1×10^{-4} to 12.7×10^{-3} m, the calculated increase in $C^{(\text{visc})}_{D,\text{forebody}}$ ranges from 18 to 30% over the range of Mach and Reynolds number encountered during the LASRE flights. Thus from Fig. 8 the expected base-pressure-drag reductions would be between 0.017 and 0.029, approximately 8–14% total reduction. These reductions are considerably larger than the minimum measurement resolution capabilities demonstrated in Fig. 5.

LASRE Drag-Reduction Experiment

In this experiment the boundary layer at the back end of the LASRE model was modified by increasing the forebody skin friction. Clearly, one of the most convenient methods of increasing the

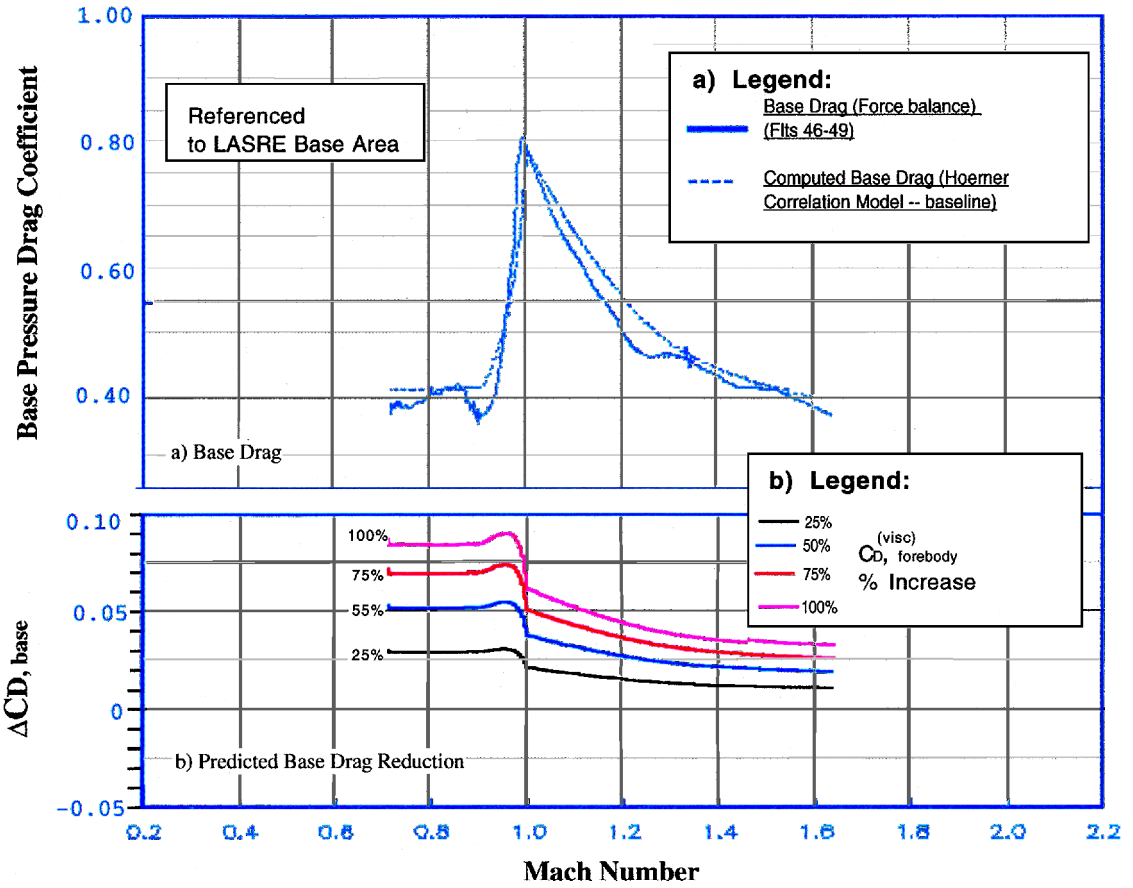

Fig. 8 Effect of viscous-forebody-drag coefficient on base-pressure-drag coefficient.

forebody skin drag is to add roughness to the surface. Other methods such as using vortex generators to energize the boundary layer would probably work more effectively, but their intrusiveness into the flow precludes this method for application to the hypersonic reentry vehicle problem. Benefits of using surface roughness are nonintrusiveness, small weight penalty, mechanical simplicity, and low cost. For the LASRE drag reduction experiment # 24 Silicon Carbide grit was glued to the skin using spray-on adhesive, and the surface was sealed using a high-tensile strength, heat resistant, white enamel paint. The resulting surface, depicted close up in Fig. 9, had an equivalent sand-grain roughness that varied from approximately 5.1×10^{-4} to 12.7×10^{-3} m. In an attempt to avoid inducing additional flow separation at the boat tail or along the forebody, only the flat sides of the LASRE model were gritted. The gritted area, also depicted in Fig. 9, covered approximately $\frac{1}{3}$ of the forebody wetted area.

Flight Results

Unfortunately, the drag-reduction experiment occurred so late in the LASRE program that only one flight test was conducted prior to the cancellation of the program. Because of this circumstance, it was not possible to verify the flight-to-flight repeatability of the experiment. Several test maneuvers were obtained during this flight, however, and a Mach range from 0.6 to 1.45 was covered. The flight results verify the effectiveness of the surface roughness technique for reducing base drag. Figure 10 shows the measured base-drag reduction compared to the predicted base-drag reduction assuming surface roughness of $(5.1 \times 10^{-4}, 12.7 \times 10^{-3}, 25.4 \times 10^{-3})$ m,

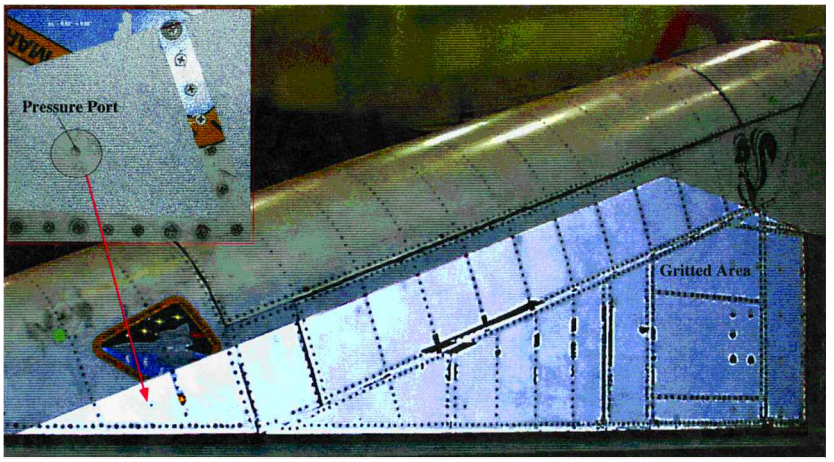

Fig. 9 Layout of the LASRE forebody grit.

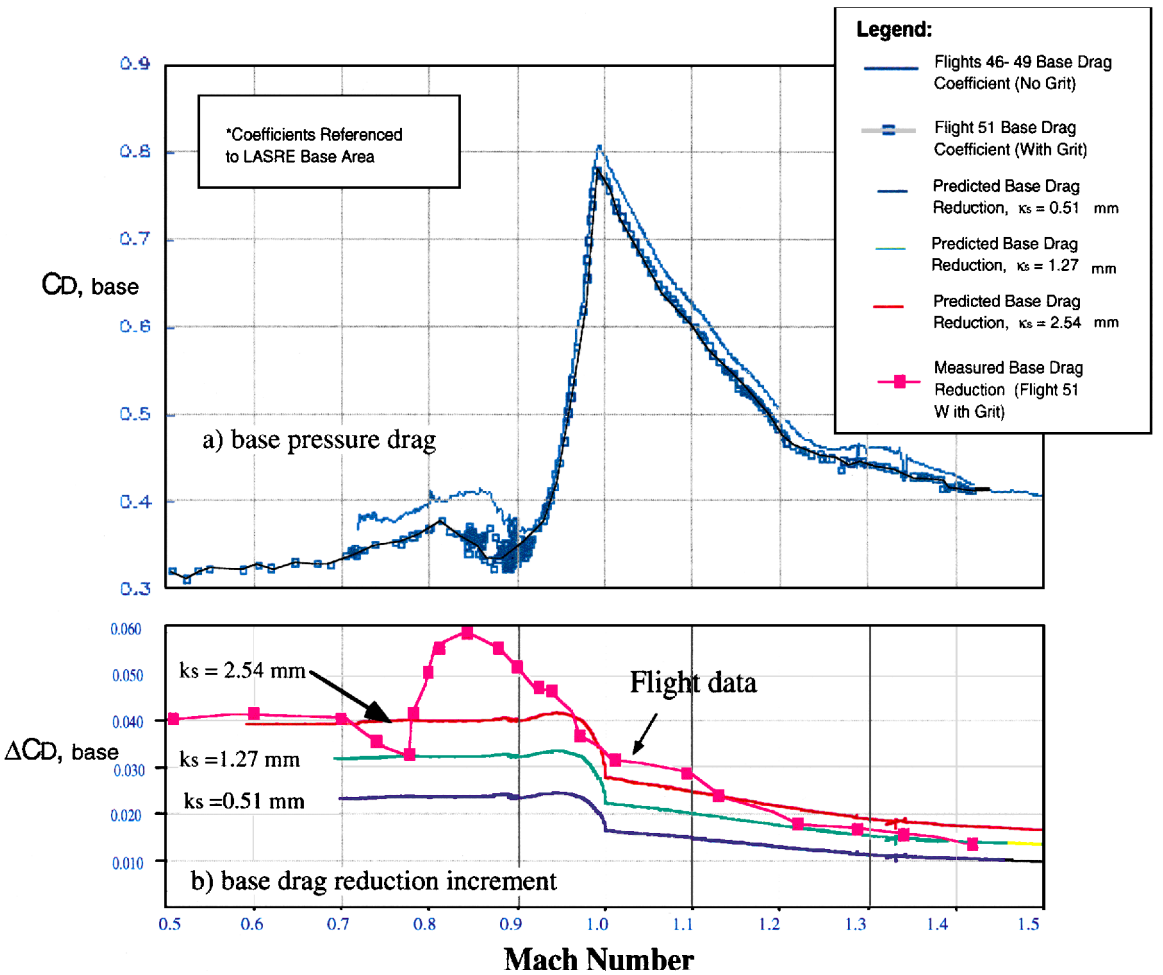

Fig. 10 Flight results, effect of forebody grit on LASRE base drag.

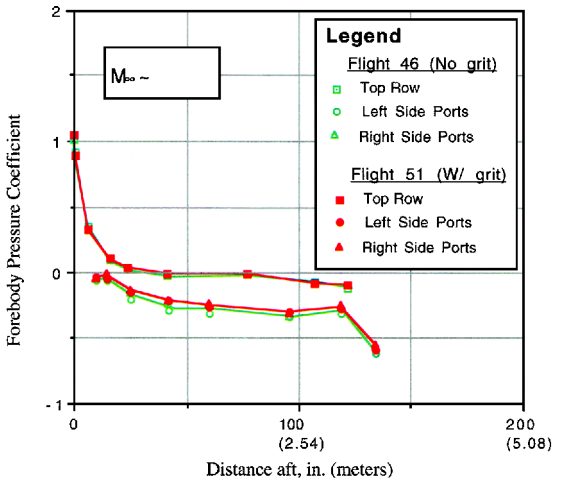

a) Pressure distribution along forebody

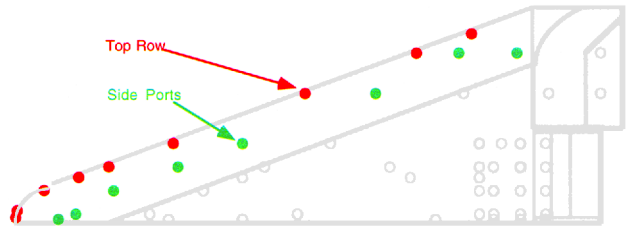

b) Side view of forebody showing pressure ports

Fig. 11 Comparison of the forebody-pressure distributions with and without grit.

respectively. Preflight calculations showed that proposed surface roughness modifications would result in base-drag reductions of 8–14%. The actual flight results showed a peak base-drag reduction of approximately 15%. The base-drag reduction also persisted well out into the supersonic flight regime. Because base drag of supersonic projectiles had never been previously correlated to viscous forebody drag, the sizable supersonic base-drag reduction was a significant positive result.

Unfortunately, the overall drag of the configuration was not reduced because the forebody grit modifications caused the forebody pressures to rise. The forebody pressures along the top and cylindrical sides of the model with and without grit are compared in Fig. 11a. The port locations for the pressures being compared are shown in Fig. 11b. These pressure data, obtained from flight 46 (no grit) and flight 51 (with grit) at Mach 0.7, are plotted as a function of the longitudinal distance aft of the nose tip. Notice that although the pressure distribution along the model centerline was basically unchanged, the pressures on the sides of the forebody are generally higher for the grit-on data. When combined with added skin drag caused by the surface roughness, the forebody pressure rise offsets the benefits gained by the base-drag reduction.

Based on these results, it must be recognized that the increase in forebody boundary-layer thickness resulting from the increased forebody drag will effect the forebody pressure distribution. Clearly the drag optimization must be modified to include not only the base-pressure-drag and viscous-forebody-drag coefficients, but must also include the forebody pressure distribution. It is likely that the relationship of forebody-pressure drag to viscous-forebody drag will be configuration dependent. Clearly, more work needs to be performed before more definite conclusions can reached. It is also clear, however, that for configurations where base drag is a dominating factor the forebody grit method is a potentially useful drag-reduction tool.

Summary and Conclusion

A drag-reduction experiment was conducted on the Linear Aerospike/SR-71 Experiment. The flight experiment performed baseline drag measurements on a clean experiment configuration. These baseline measurements were used to establish the resolution and accuracy of the measurement systems. Preflight calculations showed that the proposed surface roughness modifications would result in base-drag reductions of 8–14%, well within the resolution and accuracy limits of the measurements configuration.

Flight results verified the effectiveness of the surface roughness technique for reducing base drag. The peak base-drag reduction was approximately 15%. The base-drag reduction also persisted well out into the supersonic flight regime. Because base-drag reduction of supersonic projectiles had never been previously correlated to increased viscous forebody drag, the sizable supersonic base-drag reduction was a significant result.

Unfortunately, flight test results for rough-surface configuration did not demonstrate an overall net drag reduction. The surface grit caused a rise in forebody pressures. Coupled with increased forebody skin drag, the forebody-pressure rise offsets benefits gained by base-drag reduction. Clearly the drag optimization must be modified to include not only the base-pressure-drag and viscous-forebody-drag coefficients, but must also include the forebody-pressure distribution. Even though the drag-reduction experiment did not reduce the total vehicle drag, it is clear that, with some refinement, the forebody grit method provides a promising and useful drag-reduction tool.

References

[1]Whitmore, S. A., and Moes, T. R., "A Base Drag Reduction Experiment on the X-33 Linear Aerospike SR-71 Experiment (LASRE) Flight Program," NASA TM-1999-206575, March 1999; also AIAA Paper 99-0277, Jan. 1999.

[2]Corda, S., Lux, D. P., and Meyer, R. R., Jr., "Blackbird Puts LASRE to the Test," *Aerospace America*, Vol. 36, No. 2, 1998, pp. 25–29.

[3]Schlicting, H., *Boundary Layer Theory*, 4th ed., McGraw–Hill, New York, 1979, pp. 641, 642.

[4]Hoerner, S. F., *Fluid Dynamic Drag*, self-published work, Library of Congress Card Number 64-19666, Washington, DC, 1965, pp. 3-19, 3-20, 15-4, 16-5.

[5]Saltzman, E. J., Wang, C. K., and Iliff, K. W., "Flight Determined Subsonic Lift and Drag Characteristics of Seven Blunt-Based Lifting-Body and Wing-Body Reentry Vehicle Configurations," AIAA Paper 99-0383, Jan. 1999.

[6]Freiberger, W. F. (ed.), *International Dictionary of Applied Mathematics*, 1st ed., D. Van Nostrand Company, Inc., Princeton, NJ, 1960, p. 506.

[7]Kaplan, C., "On Similarity Rules for Transonic Flows," NACA TN-1527, Jan. 1948, pp. 8–10.

[8]Mills, A. F., and Hang, X., "On the Skin Friction Coefficient for a Fully Rough Flat Plate," *Journal of Fluids Engineering*, Vol. 105, No. 9, 1983, pp. 364, 365.

[9]Mills, A. F., *Heat Transfer*, Richard D. Irwin, Inc., Homewood, IL, 1992, pp. 282–328.

J. R. Maus
Associate Editor

Color reproductions courtesy of NASA Dryden Flight Research Center.